Supplementary Information

Ultrahigh magnetic resonance contrast switching with water gated polymer-silica nanoparticles

Daohe Yuan,[a] Connor M. Ellis,[a] Ferenc E. Mózes,[b] and Jason J. Davis*[a]

a. Department of Chemistry, University of Oxford, South Parks Road, Oxford, OX1 3QZ, UK. *E-mail: Jason.davis@chem.ox.ac.uk; Tel: +44 (0)1865 275 914*

b. Oxford Centre for Clinical Magnetic Resonance Research, Radcliffe Department of Medicine, University of Oxford, Level 0, John Radcliffe Hospital, Oxford, OX3 9DU, UK

1. Experimental

1.1 Materials

Triethanol amine (TEA) was purchased from Scientific Laboratory Supplies. 37% hydrochloric acid (HCl), N,N-dimethylformamide (DMF) and 70% nitric acid (HNO_3) were purchased from Fischer Scientific. TrypLe Express Enzyme (Gibco) and AlamarBlue cell viability reagent were purchased from Thermo Fisher Scientific. DOTA-NHS ester was purchased from CheMatech. All other chemicals were purchased from Merck and used as received. Ultrapure water (Millipore) with a resistivity of 18.2 MΩ·cm was used throughout.

1.2 Characterisation

NMR spectra were recorded by dispersing the sample (*ca.* 10 mg) in the desired deuterated solvent and acquired on a 2-channel Bruker AVIII 400 nanobay instrument running TOPSPIN 3 equipped with a 5 mm z-gradient broadband multinuclear probe. Attenuated Total Reflectance infrared (ATR-IR) spectra were recorded on an IRTracer-100 (Shimadzu) spectrometer. Ultraviolet-visible (UV-Vis) spectra were obtained using a UV-2401PC (Shimadzu) spectrometer. Fluorescence measurements were performed on a RF-6000 Spectro (Shimadzu) fluorophotometer. TEM images were obtained by FEI Tecnai 12 Transmission Electron Microscope operated at 120 kV, and the average particle diameter calculated by processing > 50 particles in ImageJ. Samples for TEM were prepared by incubating the copper grids (for 2 mins) with a drop of an aqueous colloidal suspension of the nanoparticles (*ca.* 0.5 mg/mL). Negative staining of the TEM grids was performed by incubating the prepared copper grids with 2 % uranyl acetate (for 10 s). ICP-MS measurements were performed using a PerkinElmer NexION 2000B ICP-MS spectrometer. The samples for ICP-MS were digested in 3.00 mL of concentrated (70 %) HNO_3 at room temperature for > 24 h. Then, 0.95 mL of the digested solutions were taken out and adjusted to a final volume of 50 mL using ultrapure water. The [Gd^{3+}] calibration curve was prepared using SPS-SW2 standard (Spectrapure Standards, Oslo). A Malvern Zetasizer Nano with a 532 nm laser as the light source was employed for the Dynamic Light Scattering (DLS) analysis. The samples for DLS were prepared by dispersing the nanoparticles (*ca.* 1 mg/mL) in a Britton-Robinson buffer solution (10 mM). Barrett–Joyner–Halenda (BJH) nitrogen adsorption-desorption analyses were obtained using a Micromeritics TriStar II PLUS surface characterisation analyser. Thermogravimetric analysis (TGA) was performed using a METTLER TOLEDO micro and ultra-micro balances.

Proton relaxation time measurements were acquired at 1.4 T with a Spinsolve 60 benchtop NMR (Magiterk) at room temperature. The longitudinal relaxation rate ($1/T_1$) was plotted versus the varied Gd^{3+} concentrations (in mM) with the relaxivities obtained from the slope of the associated linear fits.

Clinical MR imaging was performed on two scanners routinely used for both clinical research and to provide a cardiology service to NHS patients: these were Siemens 3 T Prisma and Siemens Avanto Fit 1.5 T systems, and both were sited in temperature-controlled, remotely monitored room. The samples were placed on the patient table with two large quality control fluid phantoms placed nearby for coil loading purposes: all imaging was undertaken using the body coil for RF transmit, and the spine array and 18-channel coils for RF receive on each scanner. After the acquisition of localisers and an automated shimming routine, shortened modified Look-Locker imaging (ShMOLLI) T_1 maps were acquired as described previously, 2 with a 192 x 144 acquisition matrix, 384 x 288 reconstruction matrix, 360 x 270 mm^2 FOV, 8 mm slice thickness, TE = 1.01 ms, TR = 2.05 ms, 35° readout flip angle, GRAPPA acceleration factor of 2 with 24 reference lines, 6/8 partial Fourier, inversion times 100 ms, 1100 ms, 2100 ms, 3100 ms, 4100 ms, 180 ms, 260 ms. The parameters of this T_1 mapping sequence match those used routinely for human cardiac imaging.

Luminescence spectroscopy was performed using a Horiba Jobin Yvon Fluorolog-3. For sample preparation, a 15 mg/mL dispersion of the pMAA-Eu-MSNs was prepared in both a D_2O and H_2O buffered solution at the desired pH. For the pH/pD 4.0 measurements, an acetate buffer solution (30 mM) was used to disperse the particles, and for pH/pD 7.0 an HEPES buffered solution (30 mM) was used. A direct excitation wavelength of 393 nm was applied on the lifetime decay measurements of time-resolved phosphorescence.

1.3 Synthesis

1.3.1 Mesoporous silica nanoparticles (Gd-MSNs)[1] with varied localisations of Gd-DOTA anchoring

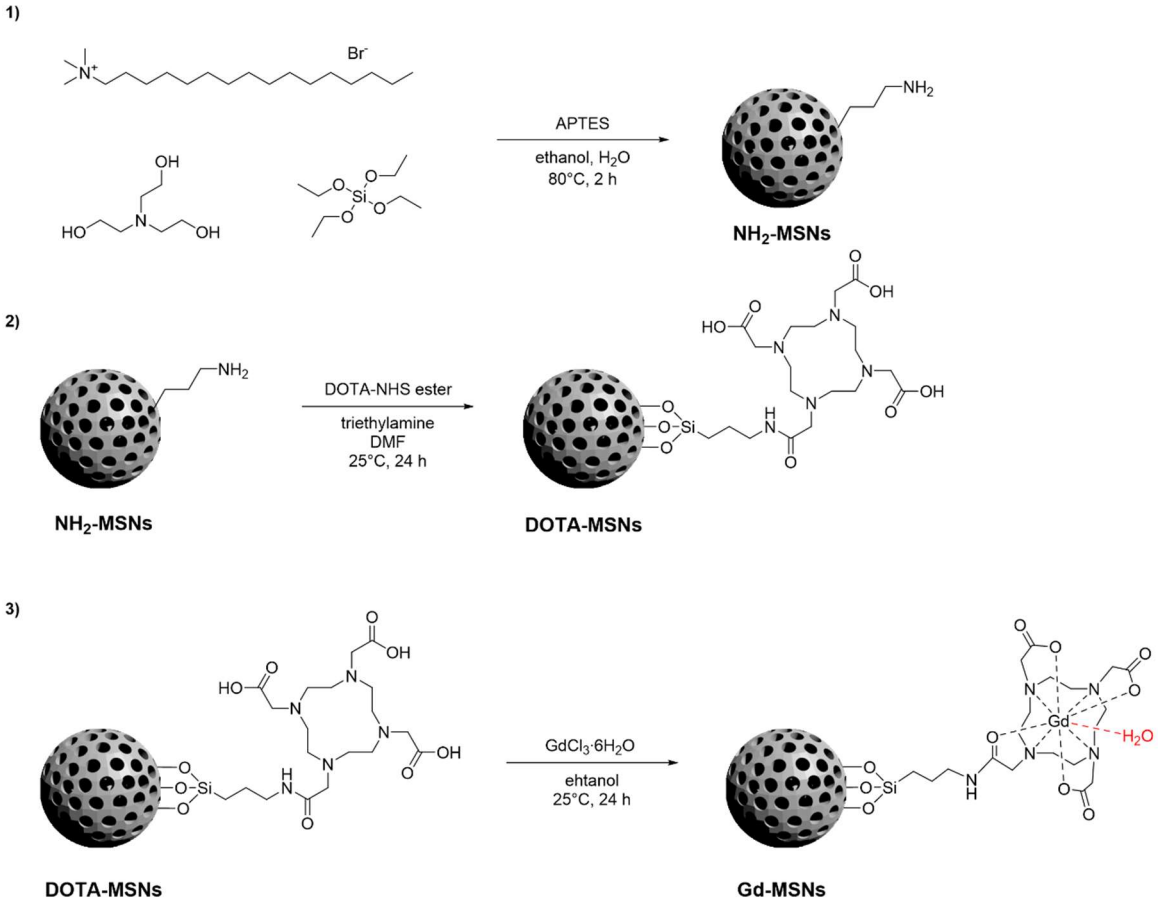

NH_2-MSNs: The syntheses of **short-delay** and **long-delay NH_2-MSNs** has been prior described in previous reports,[1] enabling the corresponding internal and peripherical modifications with Gd-DOTA.[2] For a deeper localisation of amino anchor groups (denoted as **internalised NH_2-MSNs**), a subtle modification of the co-condensation method was employed. Cetyl trimethylammonium bromide (CTAB, 0.644 g, 1.77 mmol) and triethanolamine (TEOA, 1.05 g, 7.0 mmol) were dissolved in 1.84 mL ethanol and 16.02 mL water. The temperature of the mixture was stirred at 80 °C for 20 min, allowing for complete micelle formation. Tetraethyl orthosilicate (TEOS, 1.305 mL, 5.84 mmol) was added dropwise (1 mL/ min) into the micellular solution, with the mixture vigorously stirred. After 10 mins, 3-aminopropyltriethoxysilane

(APTES, 2.34 µL, 10 µmol) was added, followed by vigorous stirring for 50 mins. TEOS (145 µL, 0.65 mmol) was then added into the reaction mixture, with another 60-min of stirring at 80 °C. The reaction mixture was allowed to cool to room temperature before collecting the nanoparticles by centrifugation (13500 rpm, 20 min). The collected pellets were re-dispersed and washed with ethanol twice, followed by re-dispersion of the nanoparticles in an acidified ethanol (10 vol% HCl) solution by sonicating for 60-min to remove any undesired surfactant template. After this acidic washing procedure, two further ethanol washing steps were performed, with the particles collected by centrifugation (13500 rpm, 20 min). The washed particles were dried under vacuum overnight.

Gd-MSNs: 200 mg of pre-dried **NH_2-MSNs** (internalised, short-delay and long-delay) were dispersed in 15 mL DMF, to which 1,4,7,10-tetraazacyclododecane-1,4,7,10-tetraacetic acid mono-N-hydroxysuccinimide ester (DOTA-NHS ester, 3.80 mg, 5 µmol) and trimethylamine (TEA, 150 µL, 1.08 mmol) were added to the MSN suspension. The reacting mixture was stirred for 24 h at room temperature. The reacted particles were collected by centrifugation (13500 rpm, 20 min) after washing three times in ethanol. The resultant nanoparticles were then re-dispersed in 10 mL EtOH. Gadolinium (III) chloride hexahydrate ($GdCl_3 \cdot 6H_2O$, 3.71 mg, 10 µmol) was added to the DOTA-MSNs suspension, with the dispersion stirred for 24 h at room temperature. The particles were collected by centrifugation (13500 rpm, 20 min) and washed three times with ethanol. The particles were dried under vacuum overnight, denoted as **internalised**, **short-delay** and **long-delay Gd-MSNs**. These Gd-MSNs have a > 98 % specificity of chelated Gd^{3+} by DOTA, as confirmed by inductively coupled plasma mass spectroscopy (ICP-MS).

1.3.2 Synthesis of 10-oxa-2-thia-5-aza-9-siladodecane(dithioic) acid, 9, 9-diethoxy-3, 3-dimethyl-4-oxo-, dodecyl ester (DDMAT-silane):[3]

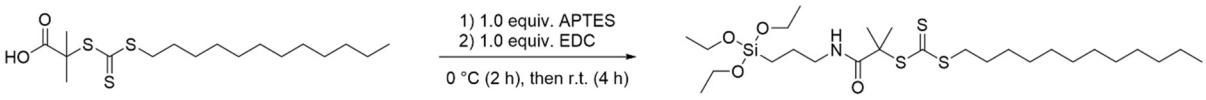

DDMAT **DDMAT-silane**

2-(Dodecylthiocarbonothioylthio)-2-methylpropionic acid (**DDMAT**, 600 mg, 1.65 mmol) was initially dissolved in DCM (50 mL). Then, *N*- (3-dimethylaminopropyl)-*N*'-ethylcarbodiimide hydrochloride (EDC) (315 mg, 1.65 mmol) was dissolved in DCM (10 mL) and subsequently added dropwise to the DDMAT solution at 0 ℃. The mixture was stirred for a further 10 mins before adding (3-aminopropyl) triethoxysilane (APTES) (385 µL, 1.65 mmol) dropwise to the flask. The reaction mixture was stirred at 0 °C for 2 h, followed by further stirring at r.t. for 4 h. The crude product was concentrated under reduced pressure, and purified by silica gel column chromatography (1:2 v/v ethyl acetate/ hexane) to yield a viscous yellow oil (**DDMAT silane**, 837 mg, yield 89 %). ^{1}H NMR (400 MHz, $CDCl_3$) δ 6.60 (H_a, t, ^3J = 5.9 Hz, 1H), 3.75 (H_b, q, ^3J = 7.0 Hz, 6H), 3.25 – 3.13 ($H_{c\text{-}d}$, m, 4H), 1.64 (H_e, s, 6H), 1.63 – 1.57 (H_f, m, 2H),

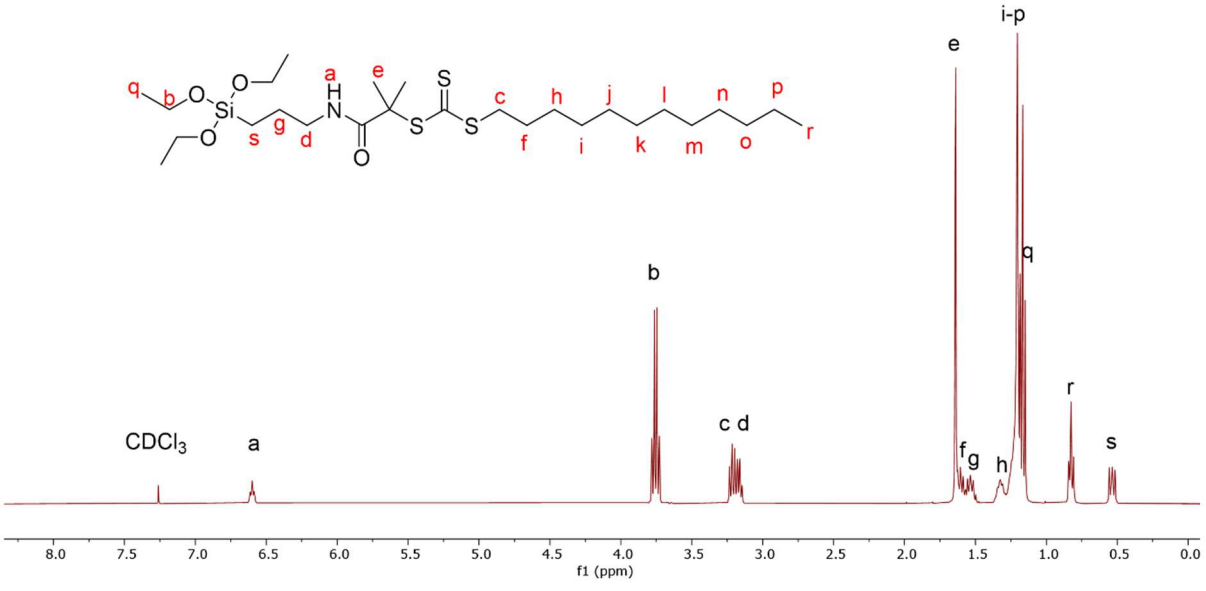

1.57 – 1.46 (H_g, m, 2H), 1.38 – 1.18 (H_{h-p}, m, 18H), 1.17 (H_q, t, ^3J = 7.0 Hz, 9H), 0.83 (H_r, t, ^3J = 6.7 Hz, 3H), 0.54 (H_s, t, ^3J = 8.0 Hz, 2H).

1.3.3 Synthesis of DDMAT modified MSNs

DDMAT-MSNs/ DDMAT-Gd-MSN: Dried native MSNs (100 mg) or Gd-MSNs (100 mg) were dispersed in an aqueous ethanol solution (v(EtOH)/ v(H_2O) = 10 mL/ 5 mL), with ammonia (800 µL) then added into the dispersion, followed by addition of DDMAT-silane (100 µL). The dispersion was stirred at 28 °C for 24 hours, followed by an ethanol washing, a DMF washing and a subsequent ethanol washing. The washed nanoparticles were collected by centrifugation (13500 rpm, 20 min) and then dried under vacuum. The grafting densities of DDMAT of the resulted nanoparticles were determined as *ca.* 4.5 groups/nm^2 by UV-Vis analyses (calculation shown below).

Control DDMAT-MSNs: dried native MSNs (100 mg) were dispersed in an aqueous ethanol solution (v(EtOH)/ v(H_2O) = 10 mL/ 5 mL), without any ammonia added to the dispersion, followed by the addition of DDMAT-silane (100 µL, 0.35 mmol). The dispersion was stirred at 28 °C for 24 hours, followed by one ethanol washing, a DMF washing and another ethanol washing. The modified nanoparticles were collected by centrifugation (13500 rpm, 20 min) and then dried under vacuum. The control nanoparticles were analysed by UV-Vis spectrometry, with no observed absorption peak at 312 nm.

1.3.4 Synthesis of polymer coated MSNs

pMAA-MSNs and pMAA-Gd-MSNs: DDMAT-Gd-MSNs or DDMAT-MSNs (50 mg) were dispersed in DMF (either 9.745 mL or 9.490 mL), with the subsequent addition of 2,2′-azobis(2-methylpropionitrile) (AIBN, 0.99 mg, 6 µmol). Before degassing with argon for 15 min, methacrylic acid (MAA, either 254 µL or 508 µL) was added to the mixture. A molar ratio of AIBN/CTA/MAA of 0.6 mM/3 mM/300 mM was denoted as the "thin-coated" polymer-silica hybrid nanoparticles, and a molar ratio of AIBN/CTA/MAA of 0.6 mM/3 mM/600 mM corresponded to the "thick-coated" nanoparticles. The fully degassed dispersions, contained in sealed reactors, were vigorously stirred at 70 °C for 18 h. The reactions were quenched by exposing to air and subsequently cooled to room temperature, with the particles then collected by centrifugation (13500 rpm, 20 min). The as-resulted nanoparticles were re-dispersed and washed three times with methanol to remove any unreacted reagents. Finally, the obtained yellow solid was dried *in vacuo* overnight for further use.

pDMAEMA-MSNs and pDMAEMA-Gd-MSNs: DDMAT-Gd-MSNs or DDMAT-MSNs (50 mg) were dispersed in DMF (either 9.495 mL or 8.990 mL), with the subsequent addition of 2,2′-azobis(2-methylpropionitrile) (AIBN, 0.99 mg, 6 µmol). Before degassing with argon for 15 min, 2-(dimethylamino)ethyl methacrylate (DMEAMA, either 505 µL or 1010 µL) was added to the mixture. A molar ratio of AIBN/CTA/DMAEMA of 0.6 mM/3 mM/300 mM was denoted as the "thin-coated" polymer-silica hybrid nanoparticles, and a molar ratio of AIBN/CTA/DMAEMA of 0.6 mM/3 mM/600 mM was denoted as the "thick-coated" nanoparticles. The fully degassed dispersions, contained in sealed reactors, were vigorously stirred at 70 °C for 18 h. The reactions were quenched by exposing to air and cooling down to room temperature, with the particles then collected by centrifugation (13500 rpm, 20 min). The as-resulted nanoparticles were re-dispersed and washed two times with DMF and one time with ethanol to remove any unreacted reagents. Finally, the obtained yellow solid was dried *in vacuo* overnight for further use.

1.4.4 Cell Viability Measurement

Cell Maintenance: Human embryonic kidney (HEK 293T) cells and HeLa cells were provided by the Nuffield Department of Clinical Neurosciences, John Radcliffe Hospital, University of Oxford. The cells were maintained in Dulbecco's Modified Eagle's Medium (DMEM, Gibco, Thermo Fisher Scientific) supplemented with 10% foetal bovine serum (FBS, Gibco, Thermo Fisher Scientific) and 1% Antibiotic-Antimycotic (FBS, Gibco, Thermo Fisher Scientific) at 37 °C with 5% CO_2 in a 95% humidified atmosphere. The medium was changed every 3–4 days, while the cells were sub-cultured after reaching about 70–80% confluency. The cells were detached with TrypLe Express Enzyme.

Cell Viability: The viability of the cells, after exposure to pMAA-Gd-MSNs, was analysed using an alamarBlue assay. Briefly, ~1 × 10^4 cells/well from each cell line were seeded in a Corning 96-well TC-

treated microplate separately in the complete medium, with three duplicate wells in each group and incubated at 37 °C in 5 % CO_2 for 24 h. Then, the cells were treated with 20µL/well of the media containing pMAA-Gd-MSNs nanoparticles to reach final concentrations of 25, 50, 75, 100, 125, 175 and 200 µg/mL. Negative control samples were prepared by treating the cells with pure media. After incubation for 24 h and 48 h at 37 °C in 5 % CO_2, the media were replaced with 100 µL/well alamarBlue cell viability reagent solution (10% alamarBlue in complete medium) and incubated protected from light at 37 °C in 5% CO_2. The plates were transferred to a microplate reader (CLARIOstar, BMG LABTECH) after further 4 h incubation. The excitation wavelength was 560 nm, and the peak at 590 nm was measured. The measured relative fluorescence units (RFU) of the wells was used to calculate the cell viability via the following equation:

$$\% \text{ Cell Viability} = \frac{Experimental\ RFU\ value\ with\ nanoparticles}{Untreated\ cell\ control\ RFU\ value} \times 100\%$$

Values were plotted by averaging duplicate wells.

2. Characterisation Figures

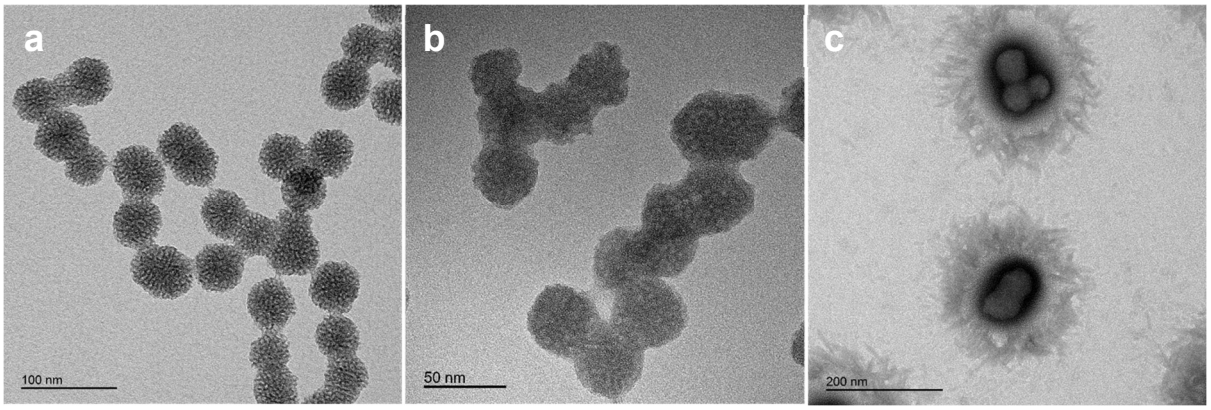

ESI 1. Transmission electron microscopy (TEM) images for the (a) bare Gd-MSNs, (b) pMAA-Gd-MSNs and (c) pDMAEMA-Gd-MSNs. Image (C) was pre-treated with a staining agent (2% uranyl acetate) prior to imaging.

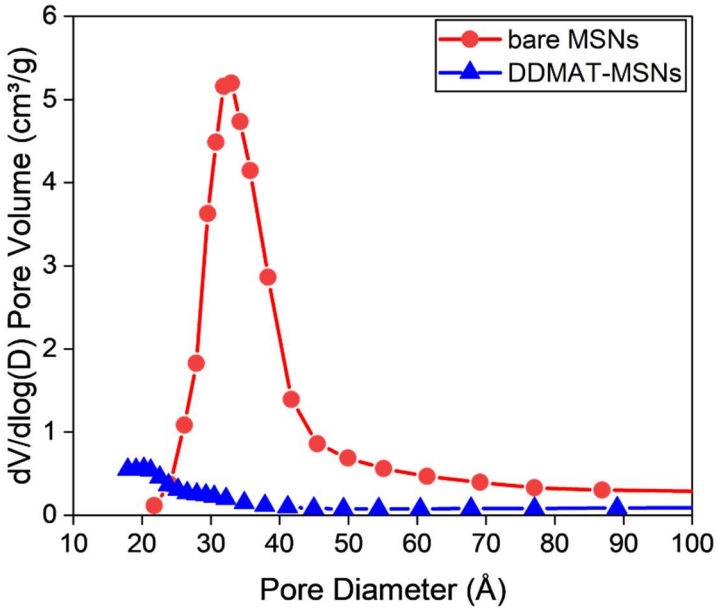

ESI 2. Barrett-Joyner-Halenda (BJH) pore size distributions for unmodified MSNs and DDMAT grafted MSNs. The average pore size of the bare MSNs is 3.2 ± 0.2 nm. The pore size of DDMAT modified MSNs is reduced to *ca.* 2.0 nm, which indicates successful external grafting of the chain transfer agent.

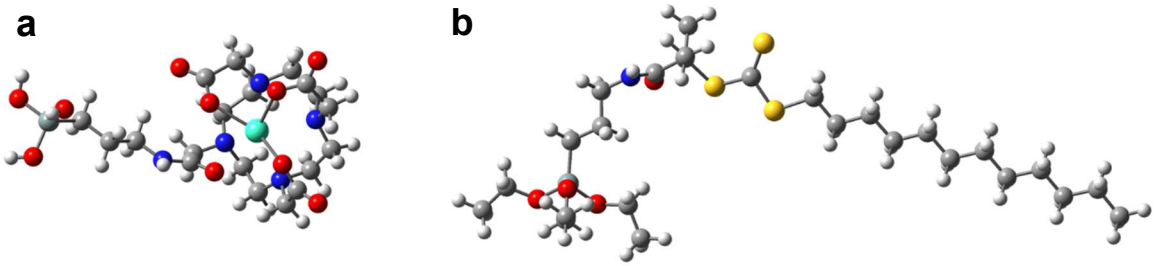

ESI 3. Optimised structure for APTES conjugated Gd-DOTA **(a)** and the optimised structure of DDMAT-silane **(b)**, by Gaussian software (with DFT b3lyp method). The optimised Gd-DOTA possess a size of 1.5 nm, with the DDMAT-silane 2.9 nm.

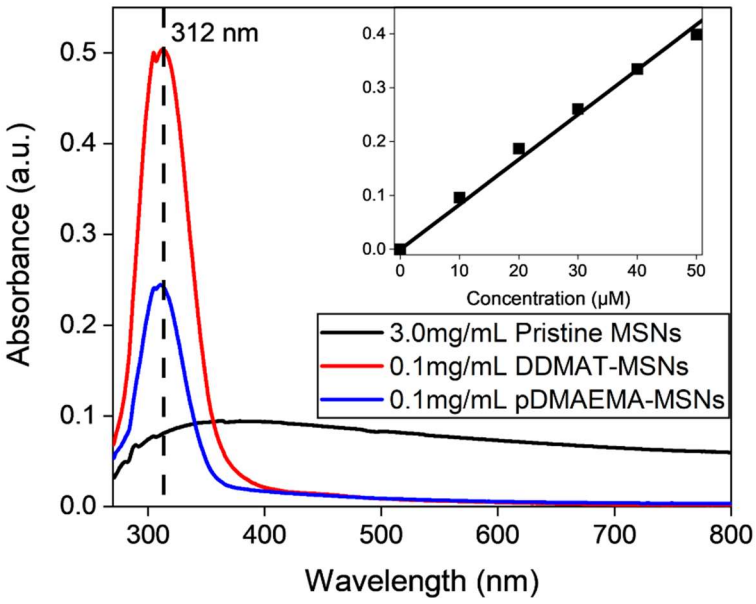

ESI 4. Ultraviolet-visible (UV-Vis) spectra for the nanoparticle dispersions in DMF, for unmodified MSNs (3.0 mg/mL), DDMAT-MSNs (0.1 mg/mL) and pDMAEMA-MSNs (0.1 mg/mL). The absorption peak at 312 nm is assigned to the trithiocarbonate group, which is employed to determine the molarity of DDMAT in the nanoparticulate dispersions. The inset shows a linear dependency between the concentration of DDMAT and the absorbance at 312 nm (in DMF).

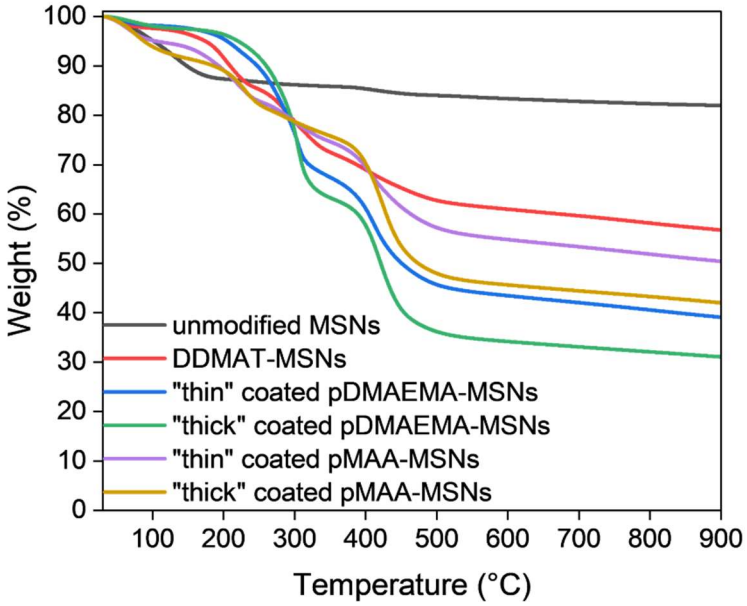

ESI 5. Thermogravimetric analyses (TGA) for different formulations of MSNs. The weight losses (at 800 °C) for DDMAT-MSNs, thin pDMAEMA-MSNs, thick pDMAEMA-MSNs, thin pMAA-MSNs, and thick pMAA-MSNs are 24.2 %, 41.8 %, 50.2 %, 30.4 %, and 39.1 %, correspondingly.

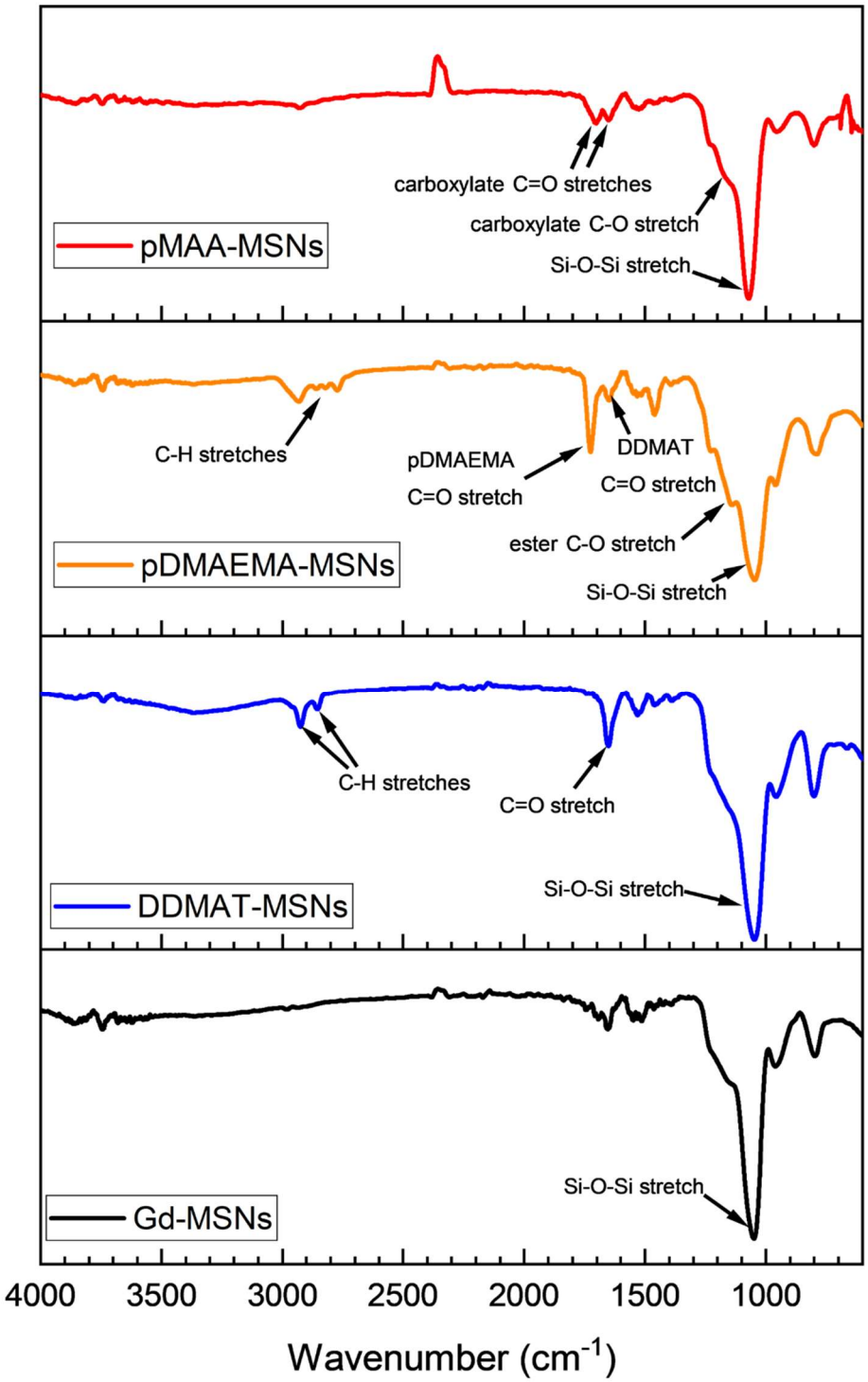

ESI 6. Infrared spectra for Gd-MSNs, DDMAT-MSNs, pDMAEMA-MSNs and pMAA-MSNs.

Concentration (c) of the nanoparticle dispersion: 1.0 mg/mL
Diameter: 50 nm
Density of MSN (ρ): 2.0 g/cm^{-3}
volume of one MSN: $V = \frac{4}{3}\pi r^3$; $V = \frac{4}{3}\pi(2.5 \times 10^{-6})^3 = 6.545 \times 10^{-17}$ cm^3
Mass of one MSN: $m = \rho V$; $m = 2.0 \times 6.545 \times 10^{-17} = 1.31 \times 10^{-16}$ g NP^{-1}
Number of MSNs per 1 mg/mL of the sample: $n = 1 \times 10^{-3} \div m$; $n = 1 \times 10^{-3} \div 1.31 \times 10^{-16} = 7.63 \times 10^{12}$ NPs
Total Surface Area of 1 mg/mL MSN sample: $A = 4 \times 7.63 \times 10^{12} \times \pi \times 25^2 = 5.99 \times 10^{16}$ nm^2
DDMAT per nm^2: $\sigma_{DDMAT} = number\ of\ grafted\ DDMAT \div A$; $\sigma_{DDMAT} = 2.695 \times 10^{17} \div (5.99 \times 10^{16}) = 4.5$ groups nm^{-2}

ESI 7. The grafting density calculation of DDMAT, by an employed literature method.[4]

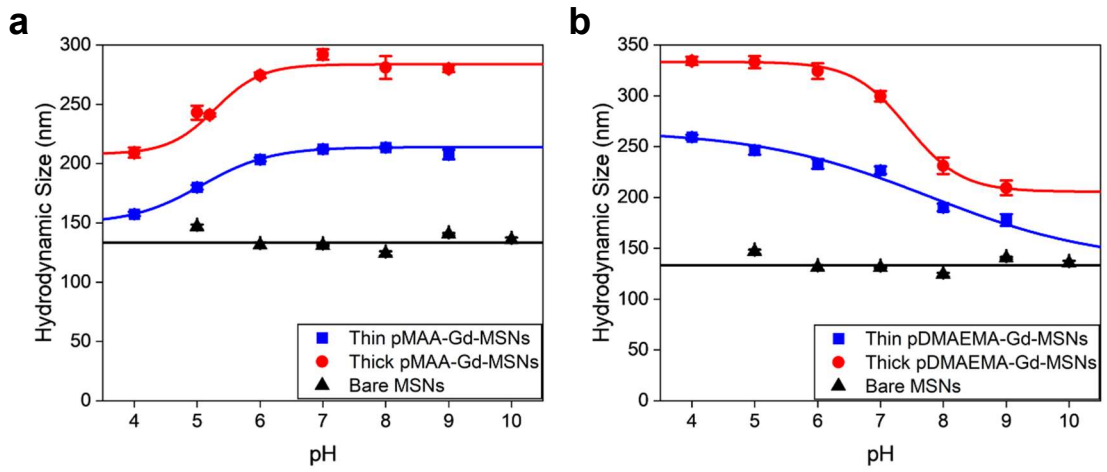

ESI 8. Dynamic light scattering (DLS) plots for pMAA-Gd-MSNs (a) and pDMAEMA-Gd-MSNs (b), compared with the unmodified MSNs. (a) The measurements for pMAA-Gd-MSNs are fitted with a Boltzmann equation to give an estimate for the pK_a = 5.1 ("thin-coated", R^2 = 0.99) and pK_a = 5.3 ("thick-coated", R^2 = 0.96). (b) The measurements for pDMAEMA-Gd-MSNs are fitted with a Boltzmann equation to give an estimate for the pK_a = 7.8 ("thin-coated", R^2 = 0.93) and pK_a = 7.4 ("thick-coated", R^2 = 0.99). The unmodified MSNs (control) show insignificant differences in hydrodynamic diameter with changes in pH, possessing an average hydrodynamic diameter (D_h) of 134.8 nm ± 7.9 nm.

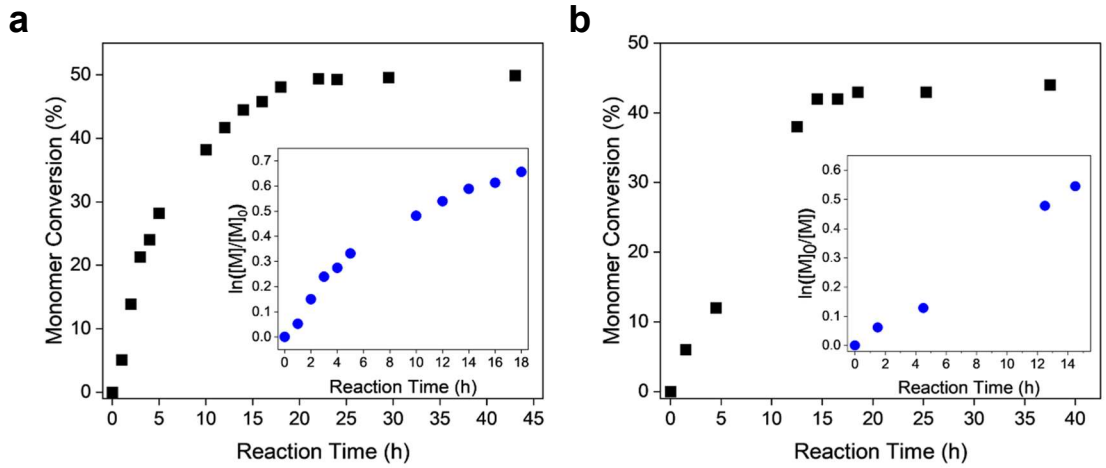

ESI 9. Monomer-conversion plots of the SI-RAFT polymerisation, measured by ^{1}H NMR, for pMAA-MSNs (a) and pDMAEMA-MSNs (b). The maximum conversions are reached after 18 h and 14.5 h, for pMAA-MSNs and pDMAEMA-MSNs, respectively. Both insets show a pseudo-first order kinetics for the SI-RAFT polymerisation of MAA (a) and DMAEMA (b).

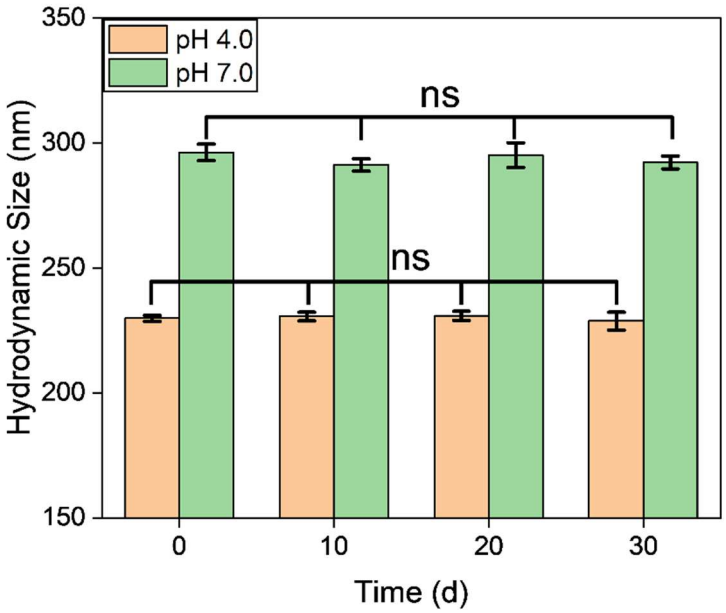

ESI 10. Stability measurements for a 1.3 mg/mL solution of the pMAA-Gd-MSNs dispersed in a Britton-Robinson buffer solution (10 mM, at pH 4.0 and pH 7.0) across a period of 30 days. As can be observed, the particles exhibit high levels of colloidal stability at both pH 4.0 and 7.0, with no significant differences in hydrodynamic size as reported by DLS analyses over the measured duration (two tailed t-test, ns, $P > 0.05$). The PDIs for all the measurements are < 0.08.

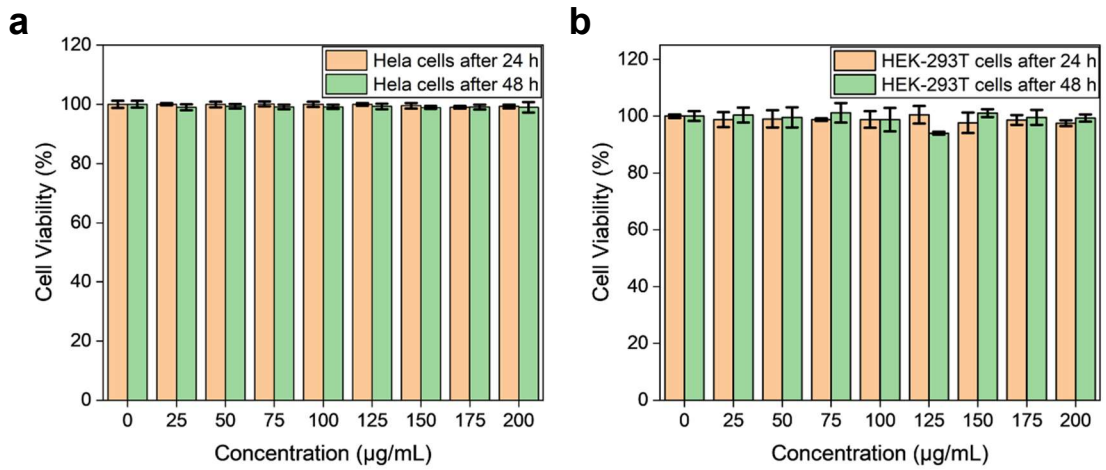

ESI 11. Cell viability tests for pMAA-Gd-MSNs with Hela cells (a) and HEK-293T human embryonic kidney cells (b).

Polymer	H-bond relaxation time (ps)	Water residence time (ps)
pDMAEMA[5]	5.40 ± 0.71 (303 K)	2.37 ± 0.20 (303 K)
pMAA[6]	*ca.* 30 (300 K)	*ca.* 10 (300 K)

ESI 12. A table comparing the relaxation times and water residence times for the defined polymer-water interactions. A neutral pH is considered for both pDMAEMA and pMAA (*i.e.* considering a protonated dimethylamino group for pDMAEMA and a deprotonated methacrylate group for pMAA). It is clear that pMAA exhibits a stronger polymer-water association in addition to a longer residence time.

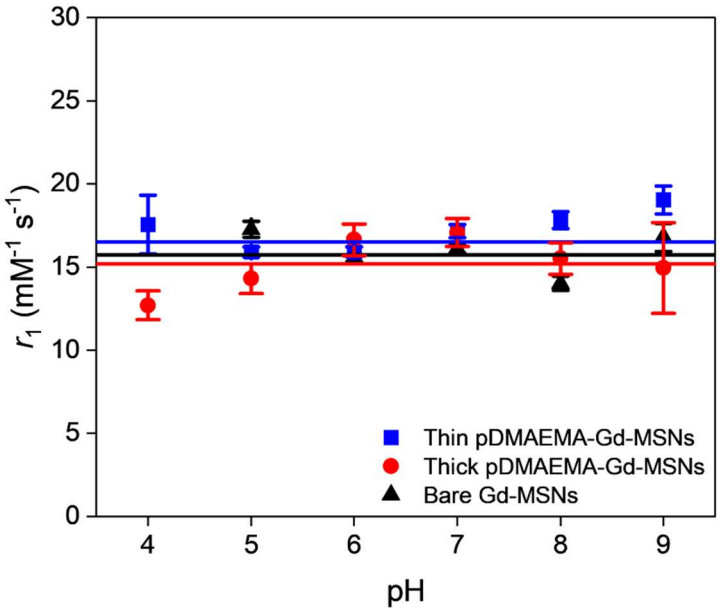

ESI 13. Comparisons of the longitudinal relaxivity values for pDMAEMA-Gd-MSNs across a full pH range with the bare Gd-MSNs. Negligible effects of the pDMAEMA shell on relaxivity is shown.

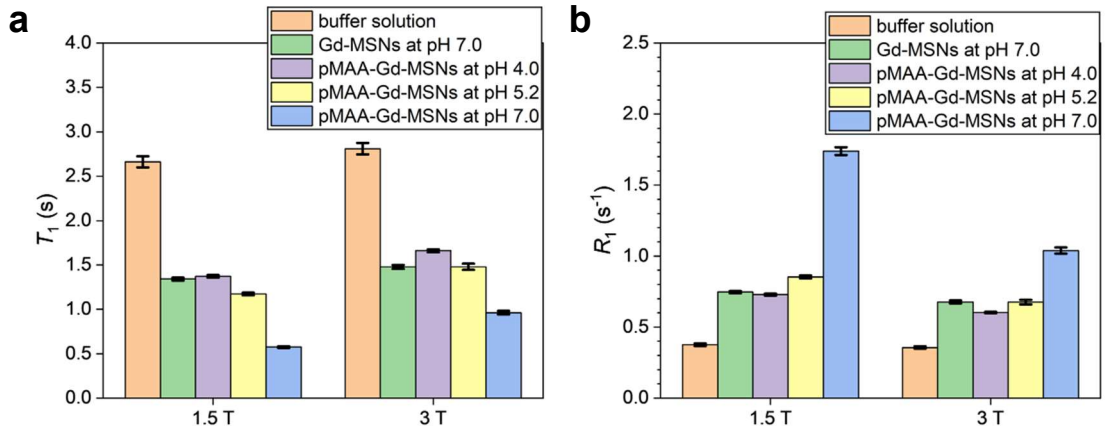

ESI 14. T_1 and R_1 values acquired from the clinical MR scanners.

ESI 15. Analysis of Solomon-Bloembergen-Morgan (SBM) theory[7]:

The observed longitudinal relaxivity (r_1^{obs}) can be written as the sum of its constituent inner-sphere relaxivity (r_1^{IS}) and outer-sphere relaxivity (r_1^{OS}) components, as shown in equation (1). The expression for r_1^{IS} is described in equation (2).

$$r_1^{obs} = r_1^{IS} + r_1^{OS} \tag{1}$$

$$r_1^{IS} = q[H_2O]/(T_{1M} + \tau_M) \tag{2}$$

where q is the number of coordinated water molecules bound to the paramagnetic ion ($q = 1$ set in this case); $[H_2O]$ is the water concentration; T_{1M} is the relaxation time of the water bound to the ion; τ_M is the residence lifetime of the inner-sphere water molecules (τ_M estimated as 480 ns[8]).

The reciprocal of T_{1M} can be expressed as the sum of the dipolar coupling relaxation rates, $1/T_1^{DD}$, the scalar interaction relaxation rate, $1/T_1^{SC}$, and the Curie spin rate, $1/T_1^{CS}$. The scalar-interaction and Curie-spin terms are often deemed to be negligible.[7] As a result, $1/T_{1M}$ is often written as the the dipole-dipole relaxation rate, $1/T_1^{DD}$.

$$\frac{1}{T_{1\mathrm{M}}} = \frac{1}{T_{1,\mathrm{DD}}} + \frac{1}{T_{1,\mathrm{SC}}} + \frac{1}{T_{1,\mathrm{CS}}} \approx \frac{2}{15}\frac{C}{r_{\mathrm{GdH}}^6}\left[\frac{F^2 3\tau_{\mathrm{cG1}}}{1+\omega_{\mathrm{I}}^2\tau_{\mathrm{cG1}}^2} + \frac{(1-F^2)3\tau_{\mathrm{cL1}}}{1+\omega_{\mathrm{I}}^2\tau_{\mathrm{cL1}}^2}\right] \tag{3}$$

$$\frac{1}{\tau_{cG1}} = \frac{1}{\tau_{RG}} + \frac{1}{\tau_M} + \frac{1}{T_{1e}} \tag{4}$$

$$\frac{1}{\tau_{cL1}} = \frac{1}{\tau_{cG1}} + \frac{1}{\tau_{RL}} \tag{5}$$

where the constant C is $\gamma_{\mathrm{I}}^2 g^2 \mu_{\mathrm{B}}^2 \left(\frac{\mu_0}{4\pi}\right)^2 S(S+1)$; γ_{I} is the proton gyromagnetic constant ($\gamma_{\mathrm{I}} = 2.675 \times 10^8$ T^{-1} s^{-1}); g is the electronic g-factor ($g = 2$ for Gd^{3+}); S is the total electron spin of the material ion (S = $7/2$ for Gd^{3+}); μ_{B} is the Bohr magneton ($\mu_{\mathrm{B}} = 9.274 \times 10^{-24}$ J T^{-1}); μ_0 is the vacuum permeability ($\mu_0 = 1.257 \times 10^{-6}$ N A^{-1}); r_{GdH} is the distance between the metal ion and the bound water proton (r_{GdH} set as 0.31 nm)[7]; ω_{H} and ω_{S} are the angular proton and electronic Larmor frequencies (with $\omega_{\mathrm{S}} = 658\omega_{\mathrm{I}}$, $\omega_{\mathrm{I}} = \gamma_{\mathrm{I}}B$, with B the magnetic field strength); F^2 denotes an order parameter that takes a value between 0 and 1; τ_{RG} is

the global correlation time; τ_{RL} is the local correlation time; τ_{cL1} is the local correlation time which accounts for fast local motion (τ_{RL}).

Here, the internal motion (*i.e.* internal flexibility of anchored Gd complex) is highlighted, which has been described by the model proposed by Lipari and Szabo.[9] Depending on the value of F^2 the motion is either governed by the global relaxation time ($F^2 = 1$) or the fast local motion ($F^2 = 0$) of the complex. In the present work, we employ the values of Gd-MSNs from those of a similar chemical structure ($F^2 = 0.5$ and $\tau_{\mathrm{RL}} = 2.4\ ns$) as described in the previous work.[8]

T_{ie} ($i = 1,2$) are given by equations (6) and (7):

$$\frac{1}{T_{1e}} = \frac{1}{25}\Delta^2\tau_v[4S(S+1)-3]\left[\frac{1}{1+\omega_s^2\tau_v^2} + \frac{4}{1+4\omega_s^2\tau_v^2}\right] \tag{6}$$

$$\frac{1}{T_{2e}} = \frac{1}{25}\Delta^2\tau_v[4S(S+1)-3]\left[\frac{5}{1+\omega_s^2\tau_v^2} + \frac{2}{1+4\omega_s^2\tau_v^2} + 3\right] \tag{7}$$

where Δ^2 (estimated at $3.8 \times 10^{19}\ \mathrm{s}^{-2}$)[10] is the mean square zero field splitting (ZFS) energy and τ_{v} (estimated at 11 ps)[10] is the correlation time for splitting.

The outer-sphere relaxivity (r_1^{OS}) is summarised by equations (8) and (9):

$$r_{1,OS} = \frac{1}{c_{Gd}}\left(\frac{1}{T_1}\right)_{OS} = \left(\frac{32\pi}{405}\right) C_{DD}\,\frac{N_A}{aD}\,Re[3j(\omega_H, T_{1e}) + 7j(\omega_S, T_{2e})] \tag{8}$$

$$j(\omega, T_{ie}) = Re\left[1 + \frac{1}{4}\left(i\omega\tau_D + \frac{\tau_D}{T_{ie}}\right)^{1/2}\right] \Big/ \left[1 + \left(i\omega\tau_D + \frac{\tau_D}{T_{ie}}\right)^{1/2} + \frac{4}{9}\left(i\omega\tau_D + \frac{\tau_D}{T_{ie}}\right) + \frac{1}{9}\left(i\omega\tau_D + \frac{\tau_D}{T_{ie}}\right)^{3/2}\right] \tag{9}$$

where Re is the real part of the spectral density function $j(\omega)$ given by equation (8), τ_D is the diffusional correlation time given by $\tau_D = a^2/D$, with D the sum of the diffusion coefficients of bulk water and the complex, and a the distance of closest approach of the water molecules to the complex (a_{GdH} set as 0.4 nm)[7].

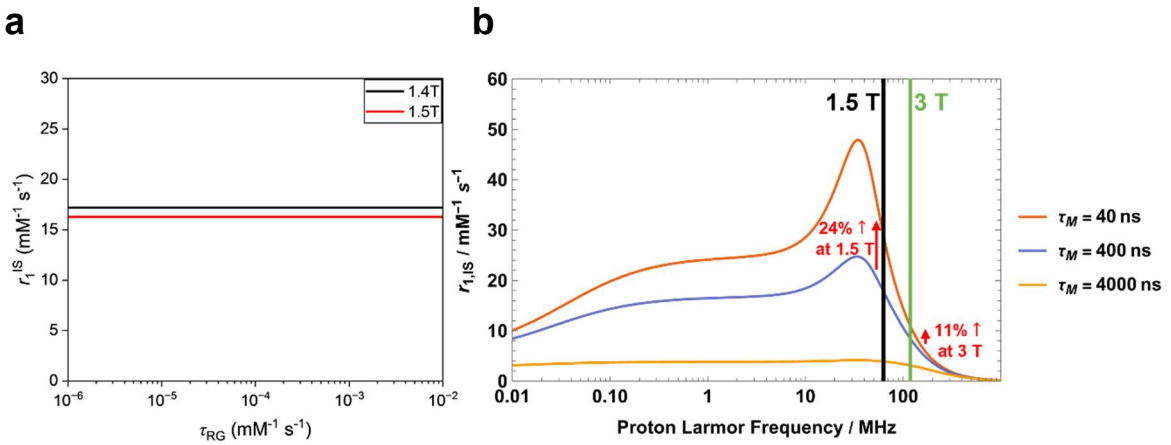

ESI 16. (a) The effects of the global rotational correlation time (τ_{RG}) on the simulated inner-sphere relaxivity ($r_{1,IS}^{sim}$), assuming an absent outer-sphere contribution. There exists no effect from the contribution of global rotation of the nanoparticles. (b) A simulated nuclear magnetic relaxation dispersion (NMRD) profile showing the effects of water exchange rate (τ_M) on $r_{1,IS}^{sim}$. The anchored DOTA-Gd complexes within a MSN scaffold have been prior reported to span a possible range of τ_M values from 40 - 1300 ns, as described in ref [8, 11 - 13]. Based on our experimental result for the unmodified Gd-doped MSNs, as well as prior literature for Gd-doped MSN analogues (ref [8, 11]), a realistic value for τ_M for our particles is on the magnitude of several hundred nanoseconds. In the simulation in (b), a wide possible range of τ_M values (40 – 4000 ns) are employed to understand differences in r_1 across this full range. Despite this, the maximum switch in τ_M (when changing τ_M from realistic values of 400 ns to 40 ns) is insignificant on comparison to the observed experimental change in r_1 (as indicated by the red arrows, $\Delta r_1\% = \Delta r_{1,IS}^{sim} / \Delta r_1^{obs} < 24\ \%$). Therefore, there is a significant additional contribution to relaxivity that is responsible for major changes in the measured relaxivity vale.

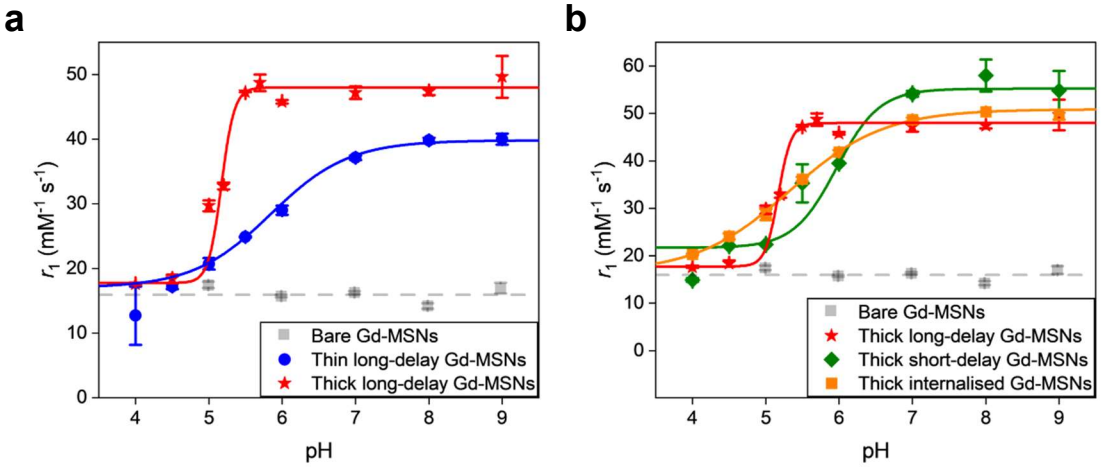

ESI 17. Longitudinal (T_1) relaxivity plots for different formulations of pMAA-Gd-MSNs, measured at 1.4 T. (a) T_1 relaxivity plot shows the effect of polymer thickness. The enhancements of r_1 are notable, with Δr_1 = 22.1 mM^{-1} s^{-1} for "thin-coated" pMAA-Gd-MSNs and Δr_1 = 30.3 mM^{-1} s^{-1} for the "thick-coated" particles. (b) T_1 relaxivity plot shows the effect of Gd-depth, where the magnitudes of the enhancement in r_1 are insignificant ("long-delay": Δr_1 = 30.2 mM^{-1} s^{-1}; "short-delay": Δr_1 = 33.5 mM^{-1} s^{-1}; "internalised": Δr_1 = 30.5 mM^{-1} s^{-1}). All relaxometric trends are fitted with a Boltzmann equation, with associated R^2 values > 0.97.

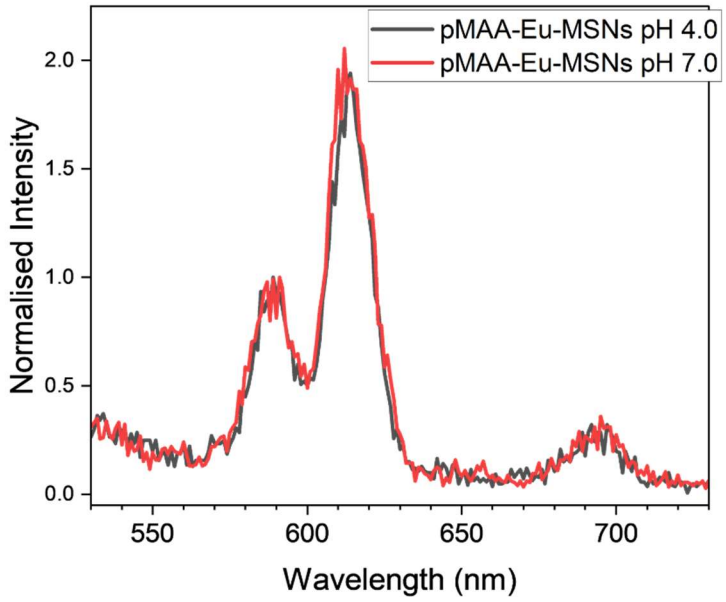

ESI 18. Normalised steady-state emission spectra of the Eu-DOTA tethered pMAA-MSNs at both pH 4.0 and pH 7.0 (in 30 mM acetate buffer for pH/pD 4.0 and 30 mM HEPES buffer for pH/pD 7.0, with λ_{ex} = 393 nm). In the spectra, the emission peaks for $^5D_0 \rightarrow {}^7F_1$ (the magnetic dipole transition peak, λ_{em} = 591 nm), $^5D_0 \rightarrow {}^7F_2$ (the induced magnetic dipole transition peak, λ_{em} = 614 nm), and $^5D_0 \rightarrow {}^7F_4$ (the induced magnetic dipole transition peak, λ_{em} = 696 nm) are pronounced. The overlapped spectra suggest that there are no conformational changes for the tethered Eu^{3+} complex, at both pH 4.0 and pH 7.0.

pMAA-Eu-MSNs	$^{a}\tau_{H_2O}$ **(ms)**	$^{b}\tau_{D_2O}$ **(ms)**
pH 4.0	0.29 ± 0.03	1.92 ± 0.19
pH 7.0	0.33 ± 0.03	2.06 ± 0.21

ESI 19. A table summarising the rate constants for the depopulation of the excited states of the pMAA-Eu-MSNs in H_2O and D_2O buffered solutions at pH 4.0 and 7.0. By monitoring the lifetime decay at λ_{em} = 591 nm ($^5D_0 \rightarrow {}^7F_1$), the corresponding decay lifetimes at both pH are shown to be within error, indicating that a constant hydration number for the tethered Eu-DOTA. ^{a,b}All luminescent lifetimes possess an intrinsic error of ± 10%.[14]

3. References

1. J. J. Davis, W. Y. Huang and G. L. Davies, *J. Mater. Chem.*, 2012, **22**, 22848-22850.
2. V. Cauda, A. Schlossbauer, J. Kecht, A. Zürner and T. Bein, *J. Am. Chem. Soc.*, 2009, **131**, 11361-11370.
3. M. Li, M. Fromel, D. Ranaweera, S. Rocha, C. Boyer and C. W. Pester, *ACS Macro. Lett.*, 2019, **8**, 374-380.
4. A. M. Santiago, T. Ribeiro, A. S. Rodrigues, B. Ribeiro, R. F. M. Frade, C. Baleizão and J. P. S. Farinha, *Eur. J. Inorg. Chem.*, 2015, **2015**, 4579-4587.
5. S. H. Min, S. K. Kwak and B.-S. Kim, *Soft Matter*, 2015, **11**, 2423-2433.
6. R. Chockalingam and U. Natarajan, *Mol. Phys.*, 2015, **113**, 3370-3382.
7. P. Caravan, C. T. Farrar, L. Frullano and R. Uppal, *Contrast Media Mol. Imaging*, 2009, **4**, 89-100.
8. F. Carniato, L. Tei, M. Cossi, L. Marchese and M. Botta, *Chem. Eur. J.*, 2010, **16**, 10727-10734.
9. G. Lipari and A. Szabo, *J. Am. Chem. Soc.*, 1982, **104**, 4546-4559.

10. L. Tei, G. Gugliotta, Z. Baranyai and M. Botta, *Dalton Trans.*, 2009, 9712-9714.
11. F. Carniato, L. Tei, J. Martinelli and M. Botta, *Eur. J. Inorg. Chem.*, 2018, **2018**, 2363-2368.
12. F. Carniato, M. Muñoz-Úbeda, L. Tei and M. Botta, *Dalton Trans.*, 2015, **44**, 17927-17931.
13. F. Carniato, L. Tei, A. Arrais, L. Marchese and M. Botta, *Chem. Eur. J.*, 2013, **19**, 1421-1428.
14. A. Beeby, I. M. Clarkson, R. S. Dickins, S. Faulkner, D. Parker, L. Royle, A. S. de Sousa, J. A. Gareth Williams and M. Woods, *J. Chem. Soc., Perkin Trans. 2*, 1999, 493-504.